separations

MDPI

Article

Chemical Microenvironments Govern Galvanically Enhanced Chlorine Activation: Molecular Probes, Ionic Effects, and Water-Matrix Control of Sunset Yellow FCF Degradation

Oualid Hamdaoui *, Abdulrahman Al-Awadi and Abdulaziz Alghyamah

Chemical Engineering Department, College of Engineering, King Saud University, Riyadh 12372, Saudi Arabia
* Correspondence: ohamdaoui@ksu.edu.sa or ohamdaoui@yahoo.fr

Abstract

The chemical environment surrounding a galvanic metal pair determines whether chlorine is productively directed toward contaminant degradation or consumed by competing constituents. This study maps those chemical microenvironments for the degradation of Sunset Yellow FCF (SSY) using a self-driven iron–copper galvanic couple in the presence of aqueous chlorine (Fe–Cu/chlorine) under a common reference condition (20 mg L^{-1} SSY, 600 µM chlorine, initial pH 5, 25 °C, 200 mL, and 400 rpm). Chloride at 10 mM shortened the degradation time to about 15 min, whereas sulfate retained near-complete degradation by approximately 24 min. In contrast, 10 mM nitrate left $C/C_0 \approx 0.38$ after 30 min, and nitrite almost completely suppressed SSY loss. Molecular probes produced differentiated responses: tert-butanol and propan-2-ol caused moderate inhibition, phenol and benzoic acid caused strong competition, nitrobenzene delayed but did not prevent the endpoint, and ascorbic acid arrested degradation. Humic acid imposed only moderate dose-dependent inhibition, with $C/C_0 \approx 0.18$ at 15 mg L^{-1} after 30 min. CO_2 bubbling gave the fastest gas-conditioned response, reaching the endpoint in about 18 min while maintaining a higher final bulk pH than the other atmospheres. In authentic waters adjusted initially to pH 5, tap water reached near-complete SSY degradation within 24 min, while tertiary-treated wastewater and Zamzam water reached $C/C_0 \approx 0.03$ and 0.12, respectively, after 30 min. By integrating ion effects, probe competition, natural organic matter, gas conditioning, and real-water performance, this work establishes the chemical microenvironment as an organizing design variable for self-powered Fe–Cu/chlorine treatment and demonstrates extensive SSY degradation across chemically diverse matrices.

Keywords: Fe–Cu galvanic coupling; chlorine-mediated oxidation; Sunset Yellow FCF; chemical microenvironment; molecular probes; humic acid; real-water matrices

Check for updates

Academic Editor: Milica Petrović

Received: 23 October 2026
Revised: 3 November 2026
Accepted: 6 November 2026
Published: 7 November 2026

Copyright: © 2026 by the authors. Licensee MDPI, Basel, Switzerland. This article is an open access article distributed under the terms and conditions of the Creative Commons Attribution (CC BY) license.

1. Introduction

Synthetic azo dyes are widely used in food, pharmaceutical, textile, and related industries, and their intense color makes even low residual concentrations conspicuous in water. Sunset Yellow FCF (SSY) is a water-soluble monoazo dye whose extended azo–aromatic conjugation produces a strong visible absorption band near 482 nm. The stability and sulfonated character of SSY can limit its removal by conventional treatment, which has motivated oxidative approaches capable of disrupting both the chromophore and the parent molecular structure [1,2].

Chlorine is an accessible oxidant already integrated into water-treatment practice. In aqueous solution, its distribution between hypochlorous acid and hypochlorite is governed

primarily by pH, while its reaction rates depend strongly on substrate structure and water composition [3]. Coupling chlorine with dissolved iron creates additional oxidation pathways. Studies of Fe(II)/chlorine systems have reported contributions from direct chlorine reactions, chlorine-centered species, and high-valent iron, with their relative importance changing with pH, iron speciation, and the target compound [4–6]. Accordingly, the reactive environment must be resolved for the specific Fe–chlorine system rather than inferred from oxidant addition alone.

A macroscopic Fe–Cu couple offers a self-driven route to supply iron species without an external power source. Electrical connection to copper renders iron the sacrificial anodic member, while the copper surface supports cathodic reactions and enlarges the effective cathodic area. The resulting galvanic current can accelerate iron dissolution and create local gradients in pH, dissolved oxygen, and redox conditions [7,8]. Integrating this electrochemical iron source with chlorine is therefore distinct from dosing soluble Fe(II): iron release, chlorine transformation, interfacial transport, and substrate oxidation evolve simultaneously within the same reactor.

The surrounding water chemistry can reorganize this coupled process. Chloride, sulfate, nitrate, and nitrite affect conductivity, iron dissolution, surface films, chlorine demand, and secondary oxidant chemistry [9,10]. Organic probe compounds can consume chlorine or short-lived oxidants, interact with dissolved iron, and perturb the metal surface. Natural organic matter introduces additional oxidant demand and metal-binding sites, whereas gas bubbling alters mass transfer, oxygen availability, carbonate equilibria, and cathodic reactions. Because these effects overlap, inhibition by one probe cannot by itself identify an exclusive reactive species [11].

Although homogeneous Fe(II)/chlorine chemistry and Fe–Cu galvanic corrosion have each been examined, the way chemically distinct microenvironments control their integrated treatment performance remains insufficiently organized. This gap is especially important for real waters, where promoting effects such as enhanced conductivity can coexist with chlorine demand, buffering, complexation, and surface passivation. A direct comparison requires a shared reactor configuration and a common reference condition.

Accordingly, this study evaluates SSY degradation by a self-driven Fe–Cu/chlorine system across five experimental tiers: inorganic ions, a chemically diverse molecular-probe set, humic acid, controlled gas atmospheres, and three authentic water matrices. All real-water experiments were adjusted initially to pH 5 to separate compositional effects from differences in starting pH.

The main contribution of this study is to connect controlled chemical perturbations with SSY degradation in authentic waters using the same self-driven Fe–Cu/chlorine configuration. Molecular-probe experiments reveal sensitivity to competing solutes and constrain possible oxidation pathways without uniquely identifying individual reactive species. Dissolved-ion experiments distinguish constituent-specific promotion, compatibility, and inhibition, demonstrating that salt addition does not produce a uniform response. Comparisons of tap water, Zamzam water, and tertiary-treated wastewater at a common initial pH establish the extent to which degradation is retained and identify matrix-dependent kinetic delays under the tested conditions. Together, these experiments provide a basis for assessing matrix compatibility and interpreting how water composition supports or suppresses treatment performance.

2. Materials and Methods

Sunset Yellow FCF (SSY; $C_{16}H_{10}N_2Na_2O_7S_2$; molar mass 452.37 g mol^{-1}; Sigma-Aldrich, St. Louis, MO, USA) was used as the target compound. Aqueous chlorine was introduced from a sodium hypochlorite solution (NaClO; approximately 13% active chlorine according

to the manufacturer's label; Chem-Lab NV, Zedelgem, Belgium) and is reported as nominal chlorine concentration. Sodium chloride, sodium sulfate, potassium nitrate, sodium nitrite, tert-butanol, propan-2-ol, phenol, nitrobenzene, benzoic acid, ascorbic acid, and humic acid were of analytical grade (Sigma-Aldrich). Working solutions were prepared with ultrapure water. Initial pH was adjusted with dilute H_2SO_4 or NaOH.

Unless otherwise stated, experiments were conducted for 30 min in an open glass batch reactor containing 200 mL of solution, with an initial SSY concentration of 20 mg L^{-1}, a nominal initial chlorine concentration of 600 μM, an initial pH of 5, a temperature of 25 °C, and a magnetic stirring speed of 400 rpm. A Fe-containing commercial steel plate and a copper plate were positioned vertically and parallel to each other, separated by 3 cm, with an immersed electrode–solution contact area of 20 cm^2 per plate. The plates were connected directly through an insulated external wire to form a spontaneous galvanic couple, without externally applied voltage or current. Before each experiment, the exposed metal surfaces were polished sequentially with silicon-carbide paper up to P4000, rinsed with ultrapure water, and dried. The required matrix constituent or probe was added according to the individual procedures described below. Immediately after chlorine addition, the electrically connected plates were immersed, defining t = 0, and aliquots were collected every 3 min. The experimental setup is illustrated in Figure 1.

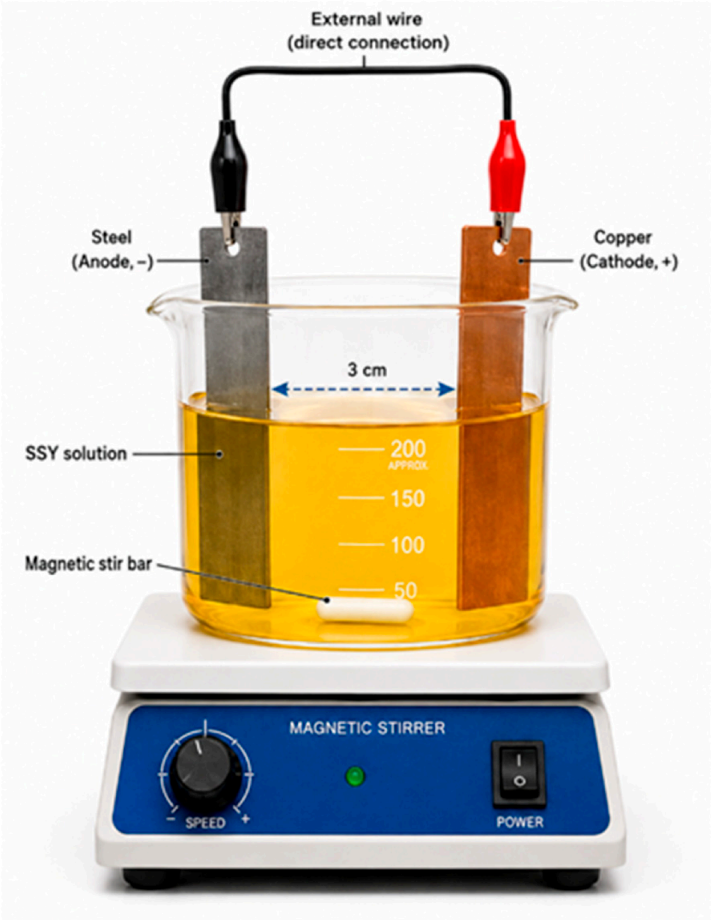


Figure 1. Experimental setup for Sunset Yellow FCF (SSY) degradation using electrically connected steel and copper plates with added chlorine (Fe–Cu/chlorine). The plates were 3 cm apart, with an immersed area of 20 cm^2 each, and connected directly by an external wire without applied voltage or current. Reference conditions: initial SSY concentration, 20 mg L^{-1}; nominal initial chlorine concentration, 600 μM; solution volume, 200 mL; initial pH, 5; temperature, 25 °C; stirring speed, 400 rpm; and treatment duration, 30 min.

The treatment labels are defined as follows: "chlorine alone" denotes an SSY solution containing added chlorine without metal plates; "Fe–Cu couple alone" denotes an SSY solution containing electrically connected steel and copper plates without added chlorine; and "Fe–Cu/chlorine" denotes an SSY solution containing both the electrically connected metal pair and added chlorine. Reference curves in the parametric experiments represent the combined Fe–Cu/chlorine treatment without the examined additive or gas bubbling, or with ultrapure water as the reference matrix.

NaCl, Na_2SO_4, KNO_3, or $NaNO_2$ was added separately at 1 or 10 mM. A salt-free run under otherwise identical conditions served as the reference.

The probe set comprised tert-butanol and propan-2-ol at 1 and 10 mM; phenol and nitrobenzene at 0.1 and 1.0 mM; and benzoic acid and ascorbic acid at 1 and 10 mM. Each probe was dissolved in the SSY solution before pH adjustment and chlorine addition. Probe responses were interpreted as integrated effects on chlorine demand, iron-mediated oxidation, adsorption, and interfacial chemistry rather than as exclusive identification of one reactive species.

Humic acid was added at 5, 10, or 15 mg L^{-1} before the initial pH was adjusted to 5. A humic-acid-free experiment served as the reference.

Separate experiments were conducted without bubbling and with continuous bubbling of N_2, O_2, CO_2, or Ar. Gas conditioning began before chlorine addition and continued throughout the 30 min reaction. Degradation and pH were measured using the same sampling schedule.

Tap water, Zamzam water, and tertiary-treated wastewater were used as authentic matrices, with ultrapure water as the reference. Each matrix was spiked to 20 mg L^{-1} SSY. Irrespective of native pH, every matrix was adjusted to initial pH 5 before addition of 600 μM chlorine.

SSY degradation was monitored by UV–visible spectrophotometry (Mettler Toledo UV7, Greifensee, Switzerland) in a 1 cm quartz cuvette at its principal visible absorption maximum near 482 nm. The normalized concentration (C/C_0) represents the apparent SSY concentration relative to its initial value and reflects decolorization at 482 nm, without establishing complete parent-dye disappearance or mineralization.

Each sample was analyzed in triplicate ($n = 3$). Results are presented as mean values, and the error bars in the figures represent the standard deviations of the three replicate measurements.

3. Results and Discussion

3.1. Inorganic Ions Reshape the Galvanic Reaction Environment

The four-ion series in Figure 2 demonstrate that added salts exert distinct effects on SSY degradation depending on their identity and concentration. In the salt-free reference, the degradation endpoint was reached at approximately 24 min. Addition of 1 mM NaCl slightly delayed the initial degradation but maintained a comparable final degradation extent and treatment time, whereas 10 mM NaCl accelerated SSY degradation, shortening the time required to reach the endpoint to approximately 15 min. Increased conductivity and chloride-sensitive iron dissolution may favor galvanic iron release, although changes in surface-film chemistry and chlorine speciation may also contribute [9].

Na_2SO_4 maintained high SSY degradation performance at both concentrations. Although degradation progressed slightly more slowly at intermediate treatment times than in the salt-free reference, a comparable final degradation extent was achieved by approximately 24 min at both 1 and 10 mM. Sulfate may improve electrical transport while modifying iron-containing surface layers; the observed response therefore indicates compatibility with the degradation process rather than intrinsic oxidative promotion.

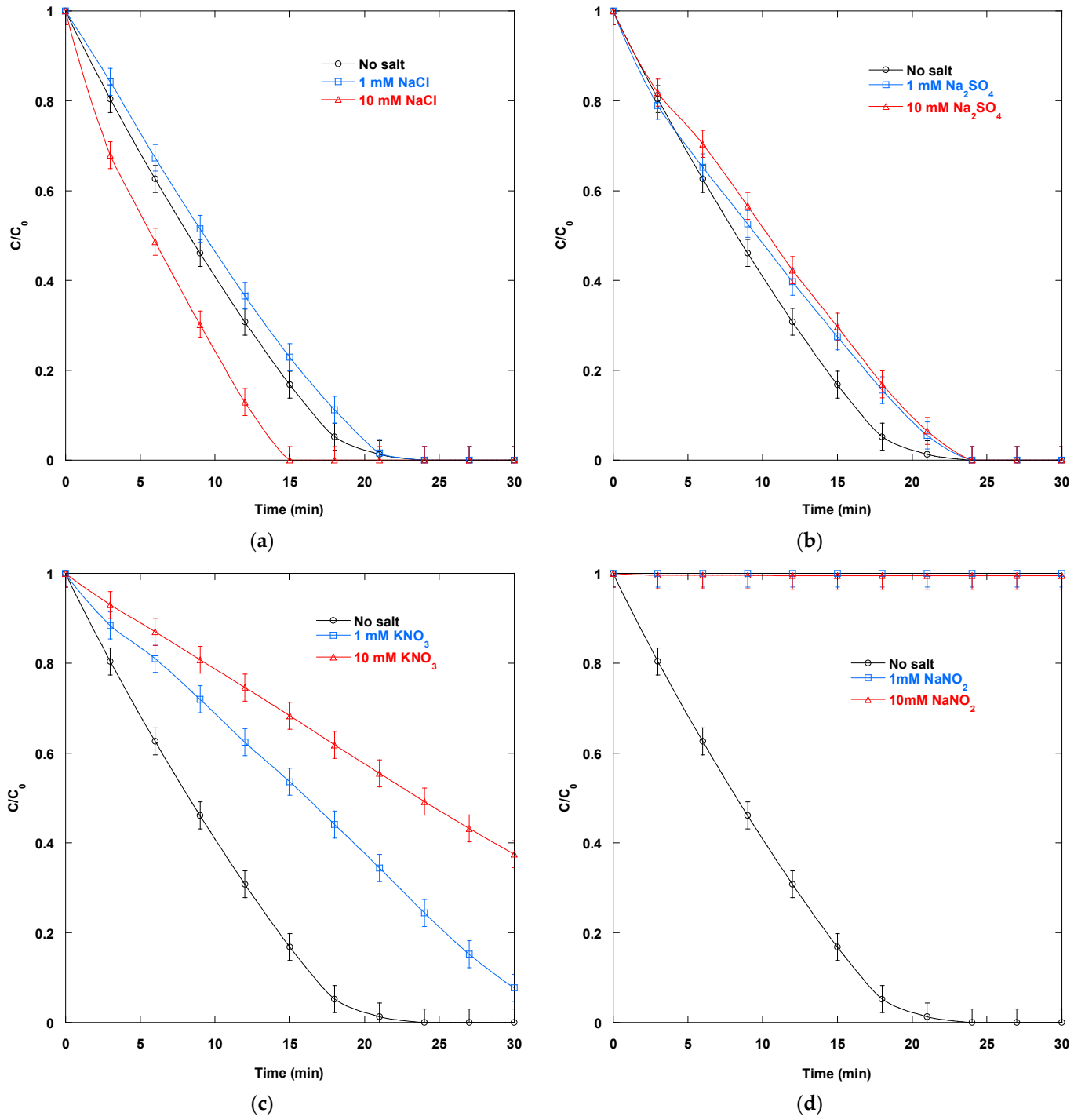


Figure 2. Effects of added inorganic ions on normalized apparent SSY concentration during Fe–Cu/chlorine treatment: (**a**) sodium chloride (NaCl), (**b**) sodium sulfate (Na_2SO_4), (**c**) potassium nitrate (KNO_3), and (**d**) sodium nitrite ($NaNO_2$). Each salt was tested at 1 and 10 mM; the salt-free experiment was the reference. SSY: Sunset Yellow FCF. Fe–Cu/chlorine: electrically connected steel and copper plates with added chlorine. Reference conditions: initial SSY concentration, 20 mg L^{-1}; nominal initial chlorine concentration, 600 μM; solution volume, 200 mL; initial pH, 5; temperature, 25 °C; stirring speed, 400 rpm; treatment duration, 30 min. C/C_0 denotes the apparent SSY concentration at each sampling time relative to its initial value. Data points represent means of three replicate measurements; error bars indicate ± one standard deviation.

KNO_3 caused clear concentration-dependent inhibition. After 30 min, C/C_0 was approximately 0.08 at 1 mM nitrate and 0.38 at 10 mM. $NaNO_2$ was far more disruptive: C/C_0 remained close to unity at both 1 and 10 mM. Nitrite reacts rapidly with free chlorine [10], so its near-complete suppression shows that preservation of the chlorine-derived oxidizing pool is essential. Overall, the ion series ranks chloride as promoting at 10 mM, sulfate as compatible, nitrate as inhibitory at high concentration, and nitrite as strongly suppressive; ionic strength alone cannot explain this order.

3.2. Molecular Probes Reveal Distributed Oxidant Reactivity

The probe screen in Figure 3 produced compound-specific concentration–response profiles. Tert-butanol and propan-2-ol, used as radical competitors, caused moderate inhibition at 10 mM, giving final C/C_0 values of approximately 0.21 and 0.17, respectively; at 1 mM, both systems retained extensive degradation. Because probe compounds can differ in reactivity, partitioning, and interfacial behavior, these alcohol responses are consistent with participation of short-lived oxidants but do not uniquely establish a hydroxyl-radical pathway [11].

The aromatic probes generated stronger but nonuniform effects. Phenol, selected as a chlorine-reactive aromatic competitor, produced dose-dependent suppression, with final C/C_0 values near 0.51 at 0.1 mM and 0.88 at 1.0 mM, consistent with its high chlorine demand and competition for oxidizing equivalents [3]. Benzoic acid, used to assess competition for transient oxidants, left C/C_0 near 0.46 and 0.62 at 1 and 10 mM, respectively; this response can include competition for transient oxidants together with perturbation of iron and interfacial chemistry. Nitrobenzene (0.1 and 1.0 mM), selected as an electron-poor aromatic comparator, behaved differently: it delayed SSY loss in a dose-dependent manner, yet both concentrations ultimately approached the baseline. Thus, early-time inhibition did not translate into a permanently lower endpoint.

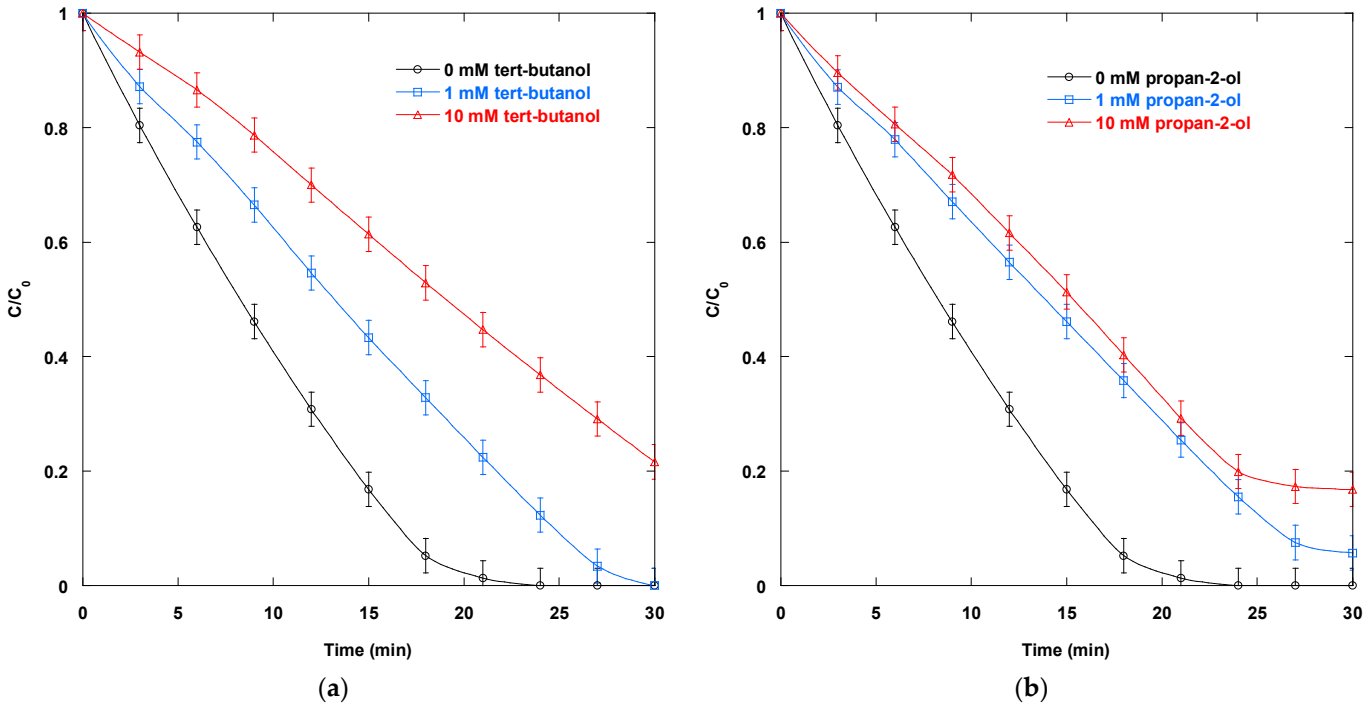


Figure 3. *Cont.*

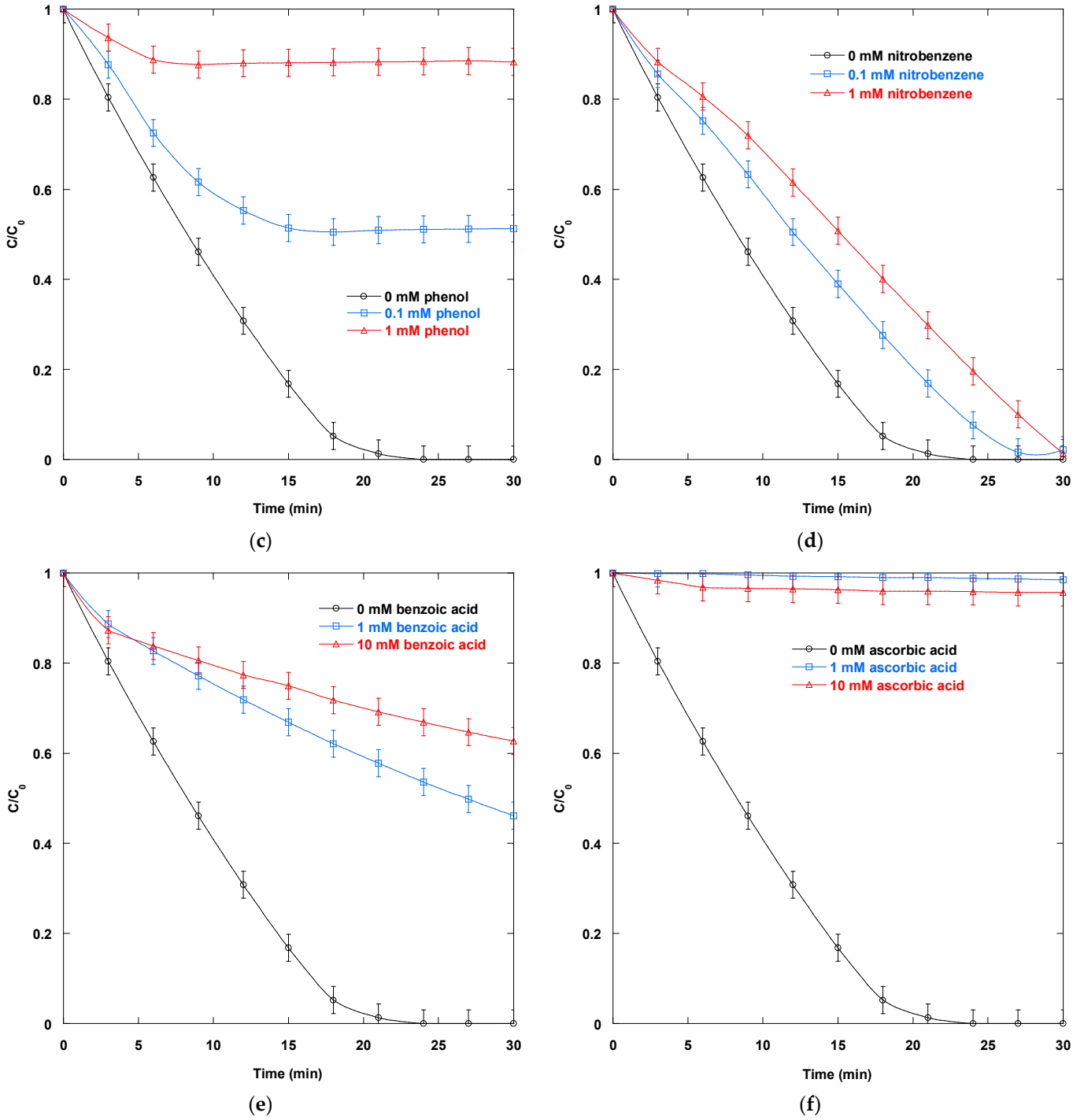


Figure 3. Effects of molecular probes on normalized apparent SSY concentration during Fe–Cu/chlorine treatment: (**a**) tert-butanol, (**b**) propan-2-ol, (**c**) phenol, (**d**) nitrobenzene, (**e**) benzoic acid, and (**f**) ascorbic acid. Concentrations were 1 and 10 mM for panels (**a**,**b**,**e**,**f**), and 0.1 and 1.0 mM for panels (**c**,**d**). Probe-free experiments were the references. SSY: Sunset Yellow FCF. Fe–Cu/chlorine: electrically connected steel and copper plates with added chlorine. Reference conditions: initial SSY concentration, 20 mg L^{-1}; nominal initial chlorine concentration, 600 μM; solution volume, 200 mL; initial pH, 5; temperature, 25 °C; stirring speed, 400 rpm; treatment duration, 30 min. C/C_0 denotes the apparent SSY concentration at each sampling time relative to its initial value. Data points represent means of three replicate measurements; error bars indicate ± one standard deviation.

Ascorbic acid, used as a reducing quencher, exerted the strongest effect, maintaining C/C_0 near unity at both 1 and 10 mM. Its ability to consume active chlorine and reduce oxi-

dizing species provides a direct explanation for the arrested response [12]. Taken together, the probe set supports a distributed reaction network involving chlorine demand, iron-mediated oxidation, and interfacial competition. The data are therefore used as comparative perturbation evidence, not as one-probe/one-species fingerprints.

3.3. Humic Acid Creates a Competitive Organic Microenvironment

Humic acid produced a progressive but moderate decrease in treatment performance (Figure 4). The humic-acid-free reference reached near-complete degradation in approximately 24 min. After 30 min, C/C_0 values were about 0.07, 0.11, and 0.18 at 5, 10, and 15 mg L^{-1} humic acid, respectively. Substantial SSY degradation was therefore retained even at the highest tested concentration.

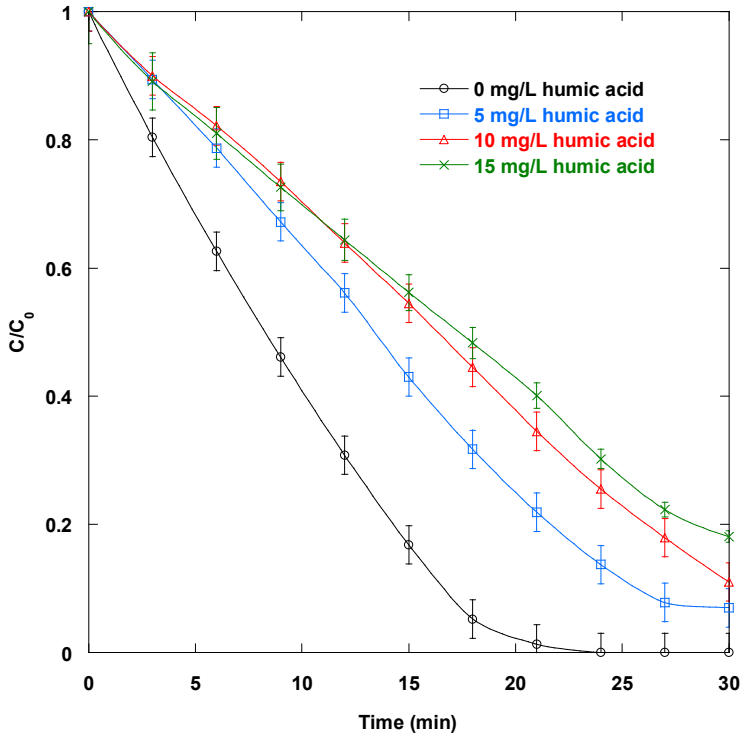


Figure 4. Effect of humic acid concentration on normalized apparent SSY concentration during Fe–Cu/chlorine treatment. Humic acid was added at 5, 10, or 15 mg L^{-1}; the humic-acid-free experiment was the reference. SSY: Sunset Yellow FCF. Fe–Cu/chlorine: electrically connected steel and copper plates with added chlorine. Reference conditions: initial SSY concentration, 20 mg L^{-1}; nominal initial chlorine concentration, 600 μM; solution volume, 200 mL; initial pH, 5; temperature, 25 °C; stirring speed, 400 rpm; treatment duration, 30 min. C/C_0 denotes the apparent SSY concentration at each sampling time relative to its initial value. Data points represent means of three replicate measurements; error bars indicate ± one standard deviation.

Humic substances can consume reactive chlorine, intercept transient oxidants, bind dissolved iron, and compete for interfacial sites [13–15]. The final pH remained within a narrow acidic range (about 3.84–3.92 with humic acid versus 4.06 in the reference), so bulk pH did not account for the dose response. The result reflects the net balance between oxidant demand and iron–organic interactions within a chemically heterogeneous organic microenvironment.

3.4. Gas Atmospheres Reconfigure the Galvanic Microenvironment

Gas conditioning affected both the SSY degradation profiles and the accompanying pH evolution (Figure 5). Without bubbling, the spectrophotometric endpoint was reached after

approximately 24 min, whereas N_2, O_2, and Ar produced broadly similar profiles with near-complete degradation after approximately 27–30 min. CO_2 showed a distinctly different response, bringing the SSY signal close to the baseline within approximately 18 min. This corresponds to an approximately 25% reduction in the time required to reach the endpoint relative to the unbubbled reference. Consequently, bubbling did not produce a uniform improvement: its effect depended on the gas introduced.

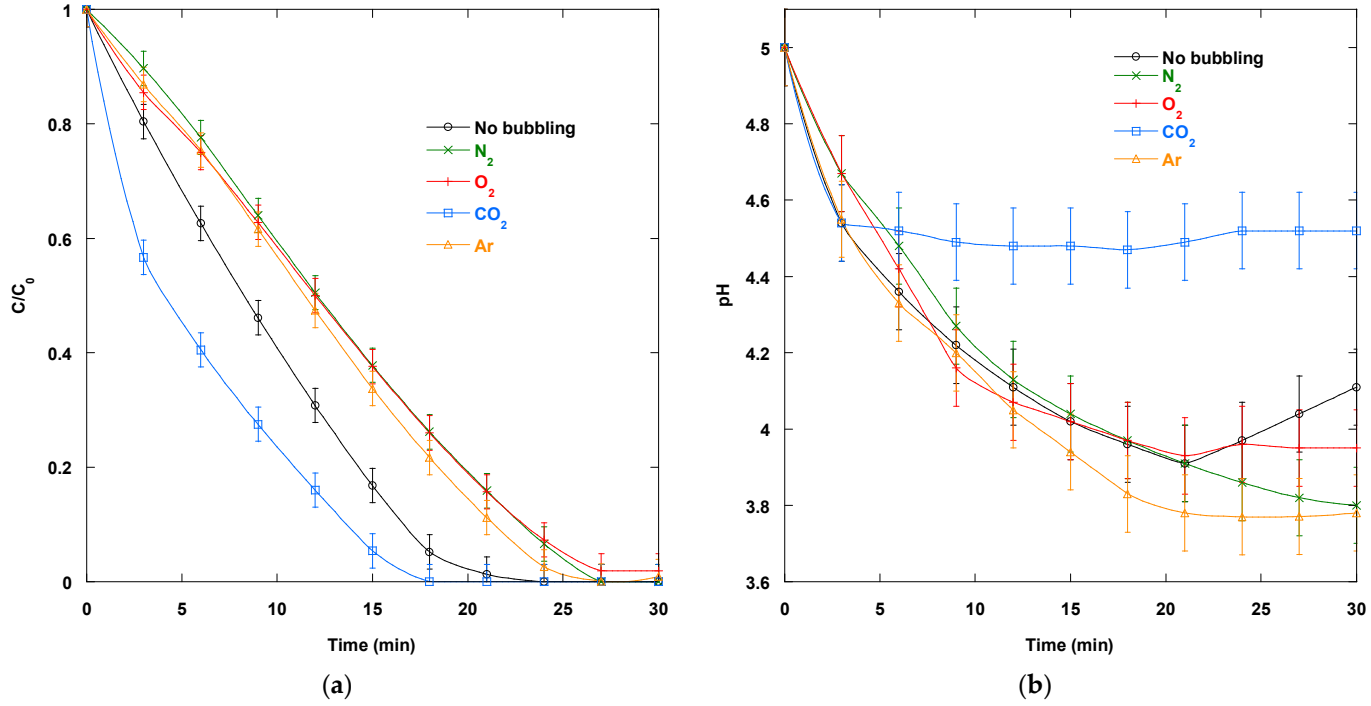


Figure 5. Effect of gas atmosphere on (**a**) normalized apparent SSY concentration during Fe–Cu/chlorine treatment and (**b**) pH evolution. Conditions were no bubbling and continuous bubbling with nitrogen (N_2), oxygen (O_2), carbon dioxide (CO_2), or argon (Ar). SSY: Sunset Yellow FCF. Fe–Cu/chlorine: electrically connected steel and copper plates with added chlorine. Reference conditions: initial SSY concentration, 20 mg L^{-1}; nominal initial chlorine concentration, 600 μM; solution volume, 200 mL; initial pH, 5; temperature, 25 °C; stirring speed, 400 rpm; treatment duration, 30 min. C/C_0 denotes the apparent SSY concentration at each sampling time relative to its initial value. Data points represent means of three replicate measurements; error bars indicate ± one standard deviation.

The similar responses under N_2, O_2, and Ar suggest that oxygen availability was not the sole factor controlling SSY degradation. Although these gases are expected to influence dissolved oxygen differently, substantial degradation was maintained under all three conditions, and O_2 bubbling provided no clear kinetic advantage over N_2 or Ar. This behavior is consistent with a chlorine-mediated oxidation process that remains effective without continuous oxygen supply. Their shared modest retardation relative to the unbubbled reference could also involve bubbling-induced changes in liquid circulation and reactant transport near the electrode surfaces. The observed profiles, however, do not separate these transport effects from changes in oxygen availability.

The pH profiles provide an important constraint on the interpretation of CO_2 promotion. Following the initial decrease, the CO_2-conditioned solution remained near pH 4.5, whereas the other systems reached approximately pH 3.8–4.1. At 3 min, the CO_2 and unbubbled experiments had comparable bulk pH values, although their SSY responses were already separated. Thus, stronger bulk acidification cannot explain the accelerated SSY signal loss under CO_2. Using a HOCl pK_a of approximately 7.54 at 25 °C [16], the calculated HOCl

fraction within the HOCl/OCl^- acid–base pair remains approximately 99.7–99.98% over pH 3.8–5.0. Changes in this distribution are therefore insufficient to explain the observed separation between the degradation profiles. Bulk pH can nevertheless influence iron dissolution, hydrolysis, and iron–chlorine reactions, so its effects on the coupled process remain relevant.

A plausible additional contribution is a CO_2-induced change in the electrochemical supply of reactive iron. Kahyarian et al. [17] demonstrated that CO_2 and associated carbonate species can modify anodic iron dissolution in acidic chloride solutions, including changes observed at controlled bulk pH. By analogy, CO_2 conditioning could alter the rate at which dissolved iron becomes available for chlorine activation, thereby changing the oxidative response without requiring a lower measured bulk pH. This interpretation connects the gas effect to the galvanic component of the process, although the corrosion conditions in that study differ from the present reactor. The higher final pH should consequently be interpreted as the outcome of the combined proton-producing and proton-consuming reactions, rather than as a direct measure of iron release or oxidizing capacity.

Overall, the results demonstrate CO_2-associated acceleration of the SSY spectrophotometric response, while N_2, O_2, and Ar retain substantial degradation with a modest delay. Gas-resolved measurements of dissolved oxygen, iron release, and galvanic current would help distinguish changes in iron availability from other effects of gas conditioning. The present data support a coupled electrochemical–chemical interpretation but do not identify the individual contribution responsible for CO_2 promotion.

3.5. Real-Water Chemistry Balances Galvanic Promotion Against Chlorine Demand

The authentic-water experiments tested whether the controlled trends persist in compositionally complex matrices (Figure 6). Each water was spiked with SSY and adjusted to initial pH 5 before chlorine addition; the native pH values in Table 1 describe the source waters and are not reaction starting values. Ultrapure water reached the spectroscopic baseline within approximately 21–24 min. Tap water followed a similarly rapid profile and reached near-complete SSY degradation at about 24 min, indicating that its moderate mineral content did not impose a prohibitive chlorine demand.

Table 1. Physicochemical characteristics of the real-water matrices compiled from published reference data [18]. Values are presented as reported in the original source; standard deviations were not determined in the present study. Native pH values are reported for characterization; every treatment experiment was adjusted to an initial pH of 5.

Parameter	Tap Water	Zamzam Water	Tertiary-Treated Wastewater
Calcium (mg L^{-1})	50	92	96
Magnesium (mg L^{-1})	15	18	28
Sodium (mg L^{-1})	90	129.5	—
Potassium (mg L^{-1})	5	44.5	—
Bicarbonate (mg L^{-1})	98	172	185
Chloride (mg L^{-1})	120	164.5	196
Sulfate (mg L^{-1})	70	123.6	—
Nitrate (mg L^{-1})	5	132.3	—
Fluoride (mg L^{-1})	0.60	0.59	—
Native pH	7.6	7.5	8.2
TDS (mg L^{-1}) [1]	350	810	1231
COD (mg L^{-1}) [1]	—	—	7
BOD_5 (mg L^{-1}) [1]	—	—	2.7

[1] TDS: total dissolved solids; COD: chemical oxygen demand; and BOD_5: five-day biochemical oxygen demand.

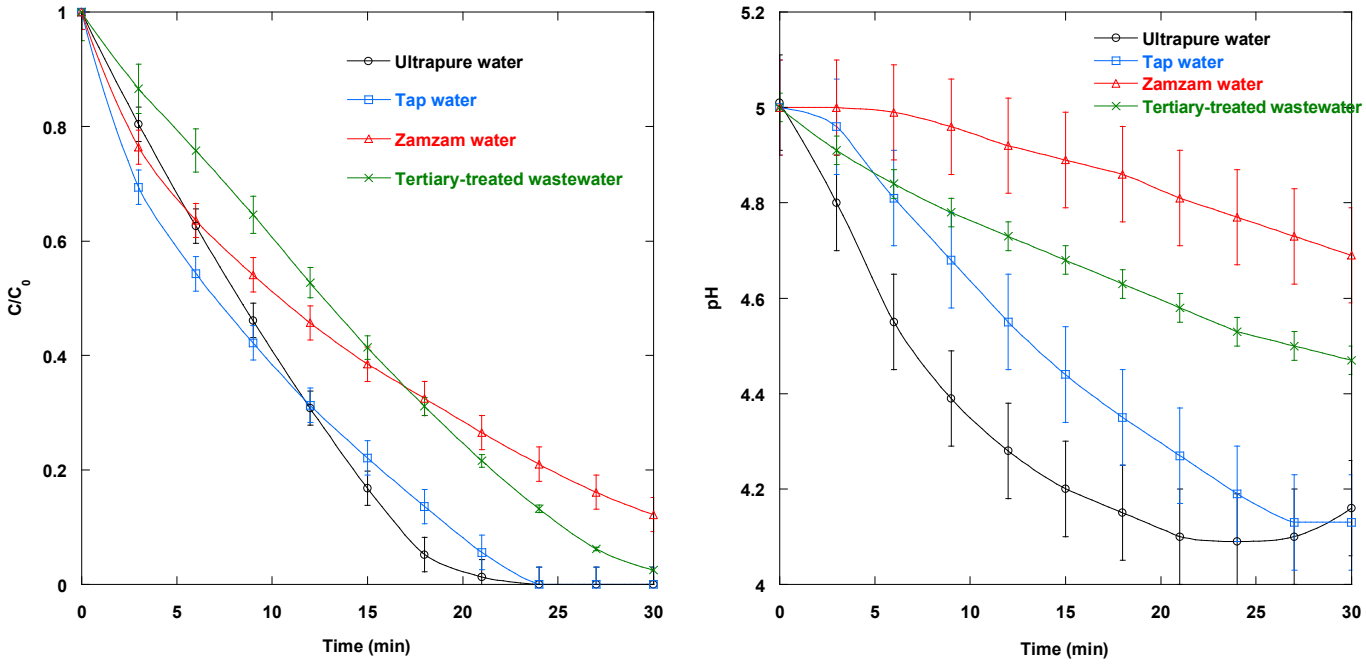


Figure 6. Fe–Cu/chlorine treatment in authentic water matrices: (**a**) normalized apparent SSY concentration and (**b**) pH evolution. Matrices were tap water, Zamzam water, and tertiary-treated wastewater, with ultrapure water as the reference. All matrices were adjusted to initial pH 5 before chlorine addition. SSY: Sunset Yellow FCF. Fe–Cu/chlorine: electrically connected steel and copper plates with added chlorine. Reference conditions: initial SSY concentration, 20 mg L^{-1}; nominal initial chlorine concentration, 600 µM; solution volume, 200 mL; initial pH, 5; temperature, 25 °C; stirring speed, 400 rpm; treatment duration, 30 min. C/C_0 denotes the apparent SSY concentration at each sampling time relative to its initial value. Data points represent means of three replicate measurements; error bars indicate ± one standard deviation.

Tertiary-treated wastewater showed a slower early response but reached $C/C_0 \approx 0.03$ after 30 min despite its TDS of 1231 mg L^{-1}, chloride concentration of 196 mg L^{-1}, bicarbonate concentration of 185 mg L^{-1}, COD of 7 mg L^{-1}, and BOD_5 of 2.7 mg L^{-1}. Zamzam water gave the highest residual response ($C/C_0 \approx 0.12$). Its elevated nitrate, bicarbonate, hardness, and total mineral content provide several simultaneous sources of kinetic resistance, including oxidant competition, buffering, and modification of iron-containing surface layers. Such combined effects are consistent with established sensitivity of iron release to chloride, sulfate, inorganic carbon, and natural organic matter [19,20].

Matrix buffering was also evident in the pH profiles. Final values were approximately 4.15 for ultrapure water, 4.13 for tap water, 4.47 for tertiary-treated wastewater, and 4.69 for Zamzam water. The more buffered matrices maintained higher pH while still allowing extensive SSY degradation. Real-water performance is thus controlled by a balance between galvanic promotion through electrolyte conductivity and competing effects from chlorine demand, nitrogen oxyanions, inorganic carbon, organic matter, and interfacial iron chemistry.

3.6. Evidence-Weighted Reactivity Map of the Fe–Cu/Chlorine Microenvironment

The complete perturbation set resolves three interacting levels of control. The galvanic level determines iron dissolution, electron flow, cathodic reactions, and surface-film development. The chlorine–iron level governs the production and consumption of the available oxidizing pool. The substrate-competition level controls how SSY competes with probe

molecules, humic matter, wastewater constituents, and transformation products. A change in water composition can act at more than one level, which explains why equal salt or probe concentrations did not yield equivalent responses.

The scavenger responses indicate that SSY degradation depends on chlorine-derived oxidizing equivalents and suggest contributions from oxidants with different selectivities. Under the acidic experimental conditions, HOCl is the predominant acid–base form of free chlorine and can participate both in direct SSY oxidation and as the precursor of iron-generated oxidants. Nitrite and ascorbic acid nearly arrested degradation at concentrations exceeding the initial chlorine concentration of 600 μM. Their strong inhibition is consistent with consumption of the available chlorine-derived oxidizing pool [10,12]. These experiments establish chlorine dependence but do not distinguish direct HOCl attack from oxidation by species generated through chlorine activation.

The alcohol and nitrobenzene experiments provide information about the scavengable component of the reaction. At 10 mM, tert-butanol and propan-2-ol left final C/C_0 values of approximately 0.21 and 0.17, respectively, while nitrobenzene delayed degradation without preventing extensive final SSY degradation. These responses are compatible with participation of short-lived oxidants, including $HO^{\bullet}$ and $Cl^{\bullet}$. However, nitrobenzene cannot be regarded as an exclusive $HO^{\bullet}$ probe because its reaction with $Cl^{\bullet}$ is also kinetically significant [11]. The persistence of substantial degradation under these conditions suggests additional oxidation pathways less effectively intercepted by the probes. Furthermore, final degradation efficiencies cannot be converted directly into percentage contributions of individual oxidants.

The stronger inhibition by the aromatic competitors further indicates differentiated oxidant reactivity. Phenol left final C/C_0 values of approximately 0.51 and 0.88 at 0.1 and 1.0 mM, respectively, consistent with its ability to compete for both free chlorine and transient oxidants. Benzoic acid produced residual C/C_0 values near 0.46 and 0.62 at 1 and 10 mM. Its stronger endpoint inhibition than nitrobenzene, including at the common concentration of 1 mM, is compatible with competition involving oxidants whose substrate selectivity differs from that of $HO^{\bullet}$ alone. Chlorine-centred radicals are therefore relevant mechanistic candidates: $Cl^{\bullet}$ generated through Fe(II)/chlorine chemistry can associate with chloride to form $Cl_2^{\bullet-}$, while secondary radical reactions involving free chlorine can generate $ClO^{\bullet}$ [5,21]. Nevertheless, the aromatic-probe responses do not resolve these species individually, and possible effects on iron speciation and interfacial reactions must also be considered.

Ferryl Fe(IV)=O provides an additional plausible oxidation pathway. Its formation in acidic Fe(II)/chlorine systems has been demonstrated independently [6], and recent work further establishes that the balance between ferryl and chlorine-radical production depends strongly on pH and chloride concentration [22]. A simplified ferryl-forming route can be represented as $Fe^{2+} + HOCl \rightarrow Fe^{IV}O^{2+} + Cl^{-} + H^{+}$. Continued SSY degradation in the presence of alcohols and nitrobenzene is compatible with an iron-oxo contribution alongside direct chlorine reactions and radical oxidation. However, these scavenger experiments do not identify ferryl directly or establish its dominance. Fe(IV)=O should therefore be included as a literature-supported candidate intermediate within the proposed chlorine–iron reaction network.

The proposed chlorine–iron reaction network also helps interpret the authentic-water results. Tap water retained rapid SSY degradation, whereas tertiary-treated wastewater showed an early delay followed by extensive removal. The slower response in Zamzam water is consistent with combined effects of nitrate, alkalinity and mineral composition on oxidant availability and iron-mediated reactions. These contrasts suggest that practical

performance reflects the balance between chlorine demand, buffering, organic competition and water constituents that influence iron dissolution and surface-film development.

The proposed reaction network is summarized schematically in Figure 7. It connects possible galvanic Fe(II) supply and chlorine activation with direct HOCl oxidation and candidate ferryl- and radical-mediated pathways. The experimental perturbation responses constrain this interpretation but do not identify individual reactive species or quantify their contributions. Accordingly, the chemical pathways are presented as literature-supported proposals.

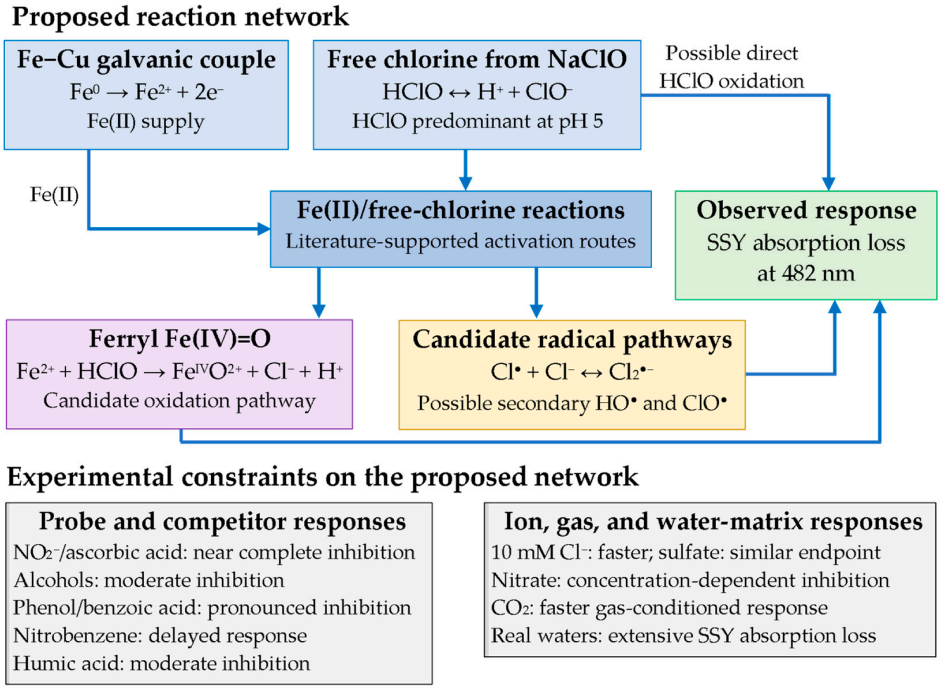


Figure 7. Proposed reaction network for Sunset Yellow FCF (SSY) transformation using electrically connected steel and copper plates with added chlorine (Fe–Cu/chlorine). The scheme integrates possible galvanic Fe(II) supply, hypochlorous acid/hypochlorite ($HOCl/OCl^-$) speciation, direct HOCl oxidation, and candidate ferryl- and radical-mediated pathways. The lower panels summarize the observed responses to probes, inorganic ions, humic acid, gas conditioning, and real-water matrices. Dashed arrows represent proposed pathways supported by the Fe(II)/chlorine literature [5,6,21,22]. Reactive-species identities and relative contributions were not established in this study. Transformation products were not identified, and mineralization was not determined.

4. Conclusions

The self-driven Fe–Cu/chlorine system exhibited pronounced sensitivity to water composition during SSY degradation. Addition of 10 mM chloride shortened the degradation time from approximately 24 to 15 min, whereas sulfate maintained extensive removal. Nitrate caused concentration-dependent inhibition, and nitrite nearly arrested degradation. Humic acid produced moderate inhibition up to 15 mg L^{-1}. Among the tested gas atmospheres, CO_2 accelerated degradation to approximately 18 min despite maintaining a higher final bulk pH, indicating that bulk acidification alone could not explain the improvement.

Alcohols caused moderate inhibition, nitrobenzene delayed the response, and phenol and benzoic acid produced stronger inhibition; ascorbic acid nearly suppressed degradation. These observations are consistent with competition involving chlorine-derived oxidants but do not establish individual reaction pathways. HOCl serves as the principal chlorine precursor under the acidic experimental conditions and may also contribute directly to SSY oxidation. Hydroxyl radicals ($HO^•$) and chlorine-centred species, including $Cl^•$ and

$Cl_2^{\bullet-}$, are plausible participants, while $ClO^{\bullet}$ and ferryl Fe(IV)=O represent additional literature-supported candidates. Their individual identities, relative contributions and dominance remain unresolved by the present scavenger experiments.

Extensive SSY degradation was retained in authentic waters adjusted initially to pH 5. Tap water reached near-complete degradation within approximately 24 min, while tertiary-treated wastewater and Zamzam water reached C/C_0 values near 0.03 and 0.12 after 30 min, respectively. These findings identify water composition as an important operating variable and provide a framework for interpreting the combined effects of oxidant competition, buffering and iron–surface chemistry on treatment performance. The main limitation for practical application is that decolorization does not establish mineralization or treated-water safety. Practical validation requires transformation-product characterization, toxicity assessment, and determination of residual chlorine and dissolved metal release.

Author Contributions: Conceptualization, methodology, formal analysis, writing—original draft preparation, writing—review and editing, supervision, project administration, and funding acquisition, O.H.; investigation, validation, data curation, and visualization, A.A.-A.; validation, visualization, and supervision, A.A. All authors have read and agreed to the published version of the manuscript.

Funding: The authors gratefully acknowledge the financial support provided by the Ongoing Research Funding Program (ORF-2026-2128), King Saud University, Riyadh, Saudi Arabia.

Data Availability Statement: Data are contained within the article.

Conflicts of Interest: The authors declare no conflicts of interest.

References

1. Gosetti, F.; Gianotti, V.; Polati, S.; Gennaro, M.C. HPLC-MS degradation study of E110 Sunset Yellow FCF in a commercial beverage. *J. Chromatogr. A* **2005**, *1090*, 107–115. [CrossRef] [PubMed]
2. Ghoneim, M.M.; El-Desoky, H.S.; Zidan, N.M. Electro-Fenton oxidation of Sunset Yellow FCF azo-dye in aqueous solutions. *Desalination* **2011**, *274*, 22–30. [CrossRef]
3. Deborde, M.; von Gunten, U. Reactions of chlorine with inorganic and organic compounds during water treatment—Kinetics and mechanisms: A critical review. *Water Res.* **2008**, *42*, 13–51. [CrossRef] [PubMed]
4. Behin, J.; Akbari, A.; Mahmoudi, M.; Khajeh, M. Sodium hypochlorite as an alternative to hydrogen peroxide in Fenton process for industrial scale. *Water Res.* **2017**, *121*, 120–128. [CrossRef] [PubMed]
5. Meghlaoui, F.Z.; Merouani, S.; Hamdaoui, O.; Alghyamah, A.; Bouhelassa, M.; Ashokkumar, M. Rapid catalytic degradation of refractory textile dyes in Fe(II)/chlorine system at near neutral pH: Radical mechanism involving dichlorine radical anion ($Cl_2^{\bullet-}$)-mediated transformation pathways and impact of environmental matrices. *Sep. Purif. Technol.* **2019**, *227*, 115685. [CrossRef]
6. Liang, S.; Zhu, L.; Hua, J.; Duan, W.; Yang, P.-T.; Wang, S.-L.; Wei, C.; Liu, C.; Feng, C. Fe^{2+}/HClO reaction produces $Fe^{IV}O^{2+}$: An enhanced advanced oxidation process. *Environ. Sci. Technol.* **2020**, *54*, 6406–6414. [CrossRef] [PubMed]
7. Gasmi, I.; Kerboua, K.; Haddour, N.; Hamdaoui, O.; Alghyamah, A.; Buret, F. Kinetic pathways of iron electrode transformations in Galvano-Fenton process: A mechanistic investigation of in-situ catalyst formation and regeneration. *J. Taiwan Inst. Chem. Eng.* **2020**, *116*, 81–91. [CrossRef]
8. Izquierdo, J.; Nagy, L.; Santana, J.J.; Nagy, G.; Souto, R.M. A novel microelectrochemical strategy for the study of corrosion inhibitors employing the scanning vibrating electrode technique and dual potentiometric/amperometric operation in scanning electrochemical microscopy: Application to the study of the cathodic inhibition by benzotriazole of the galvanic corrosion of copper coupled to iron. *Electrochim. Acta* **2011**, *58*, 707–716. [CrossRef]
9. Zhu, Y.; Zhang, J.; Wang, C.; Li, L. Effects of chloride ions and nitrate ions on the anodic dissolution of iron in sulfuric acid solution. *Metals* **2020**, *10*, 1118. [CrossRef]
10. Diyamandoglu, V.; Marinas, B.J.; Selleck, R.E. Stoichiometry and kinetics of the reaction of nitrite with free chlorine in aqueous solutions. *Environ. Sci. Technol.* **1990**, *24*, 1711–1716. [CrossRef]
11. Lei, Y.; Yu, Y.; Lei, X.; Liang, X.; Cheng, S.; Ouyang, G.; Yang, X. Assessing the use of probes and quenchers for understanding the reactive species in advanced oxidation processes. *Environ. Sci. Technol.* **2023**, *57*, 5433–5444. [CrossRef] [PubMed]
12. Bedner, M.; MacCrehan, W.A.; Helz, G.R. Making chlorine greener: Investigation of alternatives to sulfite for dechlorination. *Water Res.* **2004**, *38*, 2505–2514. [CrossRef] [PubMed]

13. Lei, Y.; Lei, X.; Westerhoff, P.; Zhang, X.; Yang, X. Reactivity of chlorine radicals ($Cl^{\bullet}$ and $Cl_2^{\bullet-}$) with dissolved organic matter and the formation of chlorinated byproducts. *Environ. Sci. Technol.* **2021**, *55*, 689–699. [CrossRef] [PubMed]
14. Gao, Y.; Jiang, J.; Zhou, Y.; Pang, S.-Y.; Ma, J.; Jiang, C.; Yang, Y.; Huang, Z.; Gu, J.; Guo, Q.; et al. Chlorination of bisphenol S: Kinetics, products, and effect of humic acid. *Water Res.* **2018**, *131*, 208–217. [CrossRef] [PubMed]
15. Li, X.; Wu, B.; Zhang, Q.; Liu, Y.; Wang, J.; Li, F.; Ma, F.; Gu, Q. Complexation of humic acid with Fe ions upon persulfate/ferrous oxidation: Further insight from spectral analysis. *J. Hazard. Mater.* **2020**, *399*, 123071. [CrossRef] [PubMed]
16. Morris, J.C. The Acid Ionization Constant of HOCl from 5 to 35°. *J. Phys. Chem.* **1966**, *70*, 3798–3805. [CrossRef]
17. Kahyarian, A.; Brown, B.; Nesic, S. Electrochemistry of CO_2 corrosion of mild steel: Effect of CO_2 on iron dissolution reaction. *Corros. Sci.* **2017**, *129*, 146–151. [CrossRef]
18. Baker, A.; Hamdaoui, O.; El Blidi, L.; Hadj-Kali, M.K.; Alghyamah, A. Ultrasound/Peracetic Acid Degradation of Sunset Yellow FCF: Scavenger-Mapped Radical Pathways and the Impact of Salts and Environmental Water Matrices. *Catalysts* **2025**, *15*, 1044. [CrossRef]
19. Lytle, D.A.; Tang, M.; Francis, A.T.; O'Donnell, A.J.; Newton, J.L. The effect of chloride, sulfate and dissolved inorganic carbon on iron release from cast iron. *Water Res.* **2020**, *183*, 116037. [CrossRef] [PubMed]
20. Peng, C.-Y.; Ferguson, J.F.; Korshin, G.V. Effects of chloride, sulfate and natural organic matter (NOM) on the accumulation and release of trace-level inorganic contaminants from corroding iron. *Water Res.* **2013**, *47*, 5257–5269. [CrossRef] [PubMed]
21. Mao, Y.; Liang, J.; Ji, F.; Dong, H.; Jiang, L.; Shen, Q.; Zhang, Q. Accelerated degradation of pharmaceuticals by ferrous ion/chlorine process: Roles of Fe(IV) and reactive chlorine species. *Sci. Total Environ.* **2021**, *787*, 147584. [CrossRef] [PubMed]
22. He, S.; Wu, Y.; Qin, W.; Li, S.; Cheng, W.; Li, P.; Wang, S.; Ouyang, G.; Zhu, M.; Fang, J. Efficient generation of highly reactive $Fe^{IV}O^{2+}$ via the Fe(II)/Cl_2 reaction for water purification. *Water Res.* **2026**, *291*, 125219. [CrossRef] [PubMed]

Disclaimer/Publisher's Note: The statements, opinions and data contained in all publications are solely those of the individual author(s) and contributor(s) and not of MDPI and/or the editor(s). MDPI and/or the editor(s) disclaim responsibility for any injury to people or property resulting from any ideas, methods, instructions or products referred to in the content.